VORTEX BREAKDOWN BEHIND POLYGONAL DISKS

Dylan Caverly
Department of Mechanical Engineering
McGill University
Montréal, Canada

dylan.caverly@mail.mcgill.ca

Jovan Nedić
Department of Mechanical Engineering
McGill University
Montréal, Canada
jovan.nedic@mcgill.ca

ABSTRACT

The influence of initial geometry on the formation, development, and decay of a vortex loop behind a polygonal disk at a Reynolds number $Re = 20,000$ is investigated. The coherence of the loop is strongest in the wake of a circular disk, remaining strong and maintaining its shape far downstream. Meanwhile, as the number of sides of the polygonal disk decrease, topological changes to the vortex loop are observed, and a faster transition to turbulence, as compared to the circular disk.

INTRODUCTION

The dynamics of coherent structures around flat plates are of particular interest in aero- and hydrodynamic applications, as they have a relationship with the drag on a body. Specifically, impulsively-started plates can be used to model biological phenomena, such as flapping wings or fins. Understanding the formation of a vortex loop and its dynamics can help us further understand and develop turbulence models, which can be used for practical design considerations, such as reducing the drag on vehicles.

Fernando & Rival (2016) investigated the forces and on impulsively-started circular and square plates at a Reynolds number of $Re = 40,000$. The transient drag forces on the square plate have a faster settling time and smaller overshoot than those on a disk. The drag forces settle to a steady-state response within a distance travelled of $s = 10l$ for the square plate, where l is the side length of the square. Meanwhile, transient drag forces on the circular plate settle beyond $s = 20l$. Using dye visualizations, they examined the structure of the vortex behind both plates. Examining the plane aligned with the primary axis of the square plate, the vortex ring formed is noted to convect further behind the square plate than the circular plate, which is noted to remain attached to the disk as far as $s = 5l$.

Higuchi *et al.* (1996) used dye visualizations to investigate the wake formation behind triangular, square, hexagonal, and octagonal plates, at Reynolds numbers $Re = 2600 - 4200$. Due to the non-uniform self-induced velocity, the initial vortex structure behind each plate was noted to be arched in the axial direction, with pairs of counter-rotating longitudinal vortices inducing inwards motion of the vortex at each corner. In the initial formation stage, individual shear layers roll up along each edge of a plate, each growing and arching until only the edges of the roll-up are connected to the corners of the disk. At this point, the individual structures combine to form one vortex loop, which eventually convects away from the plate. The vortex loop visualizations appear to contain two notable properties. First, as the number of sides of the polygonal disks increase, the vortex loop appears to be more coherent. The vortex structure breakdown occurs earlier for the triangular and square disks than the hexagonal and octagonal disks. Second, the vortex formation, and even breakdown, appear to match the dihedral group symmetry D_n of their plates. In the initial formation stage, the vortex loop maintains a similar shape to the polygonal plate, as it is still connected to the plate. However, even as the vortex structure breaks down, the dihedral symmetry remains; in the case of a square plate, a range of $0 - 45°$ is sufficient to describe the full $360°$ vortical structure, through reflections and rotations.

Similar to vortex loops generated by impulsively-started disks, previous works have studied vortex loops generated by non-circular jets (Gutmark & Grinstein, 1999; Ghasemi *et al.*, 2013). The corners of square ducts passively promote the formation of counter-rotating vortices, which promote axis switching in the vortex. The speed and location of axis switching, and subsequent transition to turbulent flow, depends on initial conditions, such as Reynolds number and initial turbulence level. Overall, geometries with sharper edges, such as triangles, circles, and rectangles, were associated with a faster transition to turbulent flow than circular or oval nozzle geometries (Grinstein & DeVore, 1996).

The effects of geometry for a steady turbulent wake were examined by Nedić *et al.* (2015) at Reynolds number $Re = 82,000$. Using pairs of hot-wire measurements at a fixed radial distance, they extracted azimuthal energy at the radial distance where vortex energy is at its strongest. They found that the relative amount of fluctuating energy contained in the $m = 1$ mode depends on flat plate geometry. For example, at $x = 10l$,
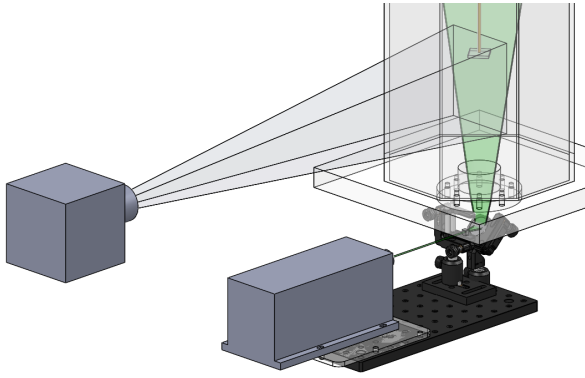
Figure 1.   Rendering of the experimental setup.

Table 1.   Plate properties .

Shape	$\sqrt{A}$ (mm)	P (mm)	D_h (mm)
Circle	35.4	125.3	39.9
Hexagon	35.4	131.6	38.0
Pentagon	35.4	134.8	37.1
Square	35.4	141.4	35.4
Triangle	35.4	161.2	31.1

Figure 2.   Top view of triangular plate and coordinate system of experimental setup.

where $l = \sqrt{A}$ is the square root of the area of the plate, the relative amount of fluctuating energy in the $m = 1$ mode is 73% for a disk, while for fractal plates, it decreases from 63% to 55% with increasing fractal iteration.

Geometry is also known to affect the steady drag force on plates. Nedić *et al.* (2015), for example, demonstrated that plates with the same frontal area, but with higher fractal geometry (therefore more complex perimeter geometry) had larger drag coefficients. For impulsively started flows, Fernando *et al.* (2020), measuring circular disks, found that inviscid added-mass models do not alone account for the total forces on disks during impulsive motions, underestimating resultant forces by 20% at high accelerations. Additional models must, therefore, be developed to accurately estimate residual forces.

The vast majority of our understanding of the underlying dynamics of vortex formation and decay to turbulence comes from studying circular disks. In this study, we are interested to discover to what degree the initial geometry of a body generating a vortex loop has on the large-scale structures that are generated. Specifically, our objective here is to determine the geometry and coherence of the initial vortex loop behind a plate as it breaks down into turbulence, and to understand what aspects of the initial geometry drive any observed changes. Moreover, understanding the nature of the generated turbulence, and relating that to the geometry and initial conditions, would help understand how these conditions can be controlled.

EXPERIMENTAL SETUP

Experiments were performed in an acrylic octagonal water tank with a circumscribed diameter of 200 mm, with a rendering provided in fig. 1. A set of circular and polygonal plates (triangle, square, pentagon and hexagon) was pulled vertically by a servocylinder from rest at a constant acceleration rate of 12.5 mm/s^2, to a steady-state velocity of $U = 750$ mm/s. The servocylinder has a maximum stroke length of 300 mm. Each plate has a thickness of 3 mm and area of $A = 1250$ mm^2, therefore with corresponding characteristic length $l = \sqrt{A} = 35.4$ mm. Using the steady-state plate speed as a characteristic velocity, the experiment has an associated Reynolds number of $Re = 27,000$. Plate properties are shown in table 1. While all plates have the same area of $A = 1250$ mm^2, as the number of sides decreases, the sharpness of the discontinuities therefore increases, and the plate perimeter increases from $P = 125.3$ mm for the circular plate to $P = 125.3$ mm for the triangular plate.

Images were gathered using two Photron Fastcam Mini
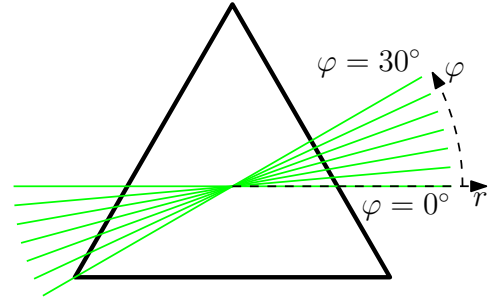
WX50 cameras at a rate of 1500 s^{-1}. Using Particle Image Velocimetry (PIV) with DaVis 10.1.0, vorticity was calculated in the region surrounding the plate in a plane at a fixed angle φ in a range $(r/l, x/l) \in [-1.5, 1.5] \times [-0.25, 4.25]$. The coordinate system is provided in fig. 2, using a cylindrical $r - \varphi - x$ coordinate system, with the plate travelling a distance s in the x-direction. Measurements were performed in $r - x$ planes in increments of $\varphi = 5°$. Five repeats were performed for each plate at each orientation.

Due to the D_n dihedral symmetry of each polygonal plate, and assumed symmetry of each vortex loop, PIV was only performed in the range of the fundamental domain of each plate. For example, behind a triangular disk, experiments were performed at azimuthal angles $\varphi \in [0°, 60°]$, which, with sufficient rotations and reflections, can describe the full $360°$ field. Due to the PIV setup, these experiments also captured results at $\varphi \in [180°, 240°]$, with corresponding ranges for all other plates.

BULK FLOW RESULTS
Circulation

Circulation Γ behind each plate is plotted in fig. 3, with a circular marker denoting the point where the plate transitions from constant acceleration to constant velocity. Circulation is calculated by integrating the vorticity field behind each plate in the half-plane, over $(r, x) \in [0, l] \times [-0.25l, x_{\text{plate}}]$, and averaging the field circulation over all measured azimuthal angles. Geometry does not appear to play a major role on the circulation of the vorticity field, as circulation patterns for all shapes collapse to approximately the same curve.

The circulation being self-similar across all plates is consistent with existing literature; from an added-mass perspective, since all plates have the same area, the same volume of fluid is displaced by each plate. With the same volume of fluid displaced, the same amount of circulation is introduced into
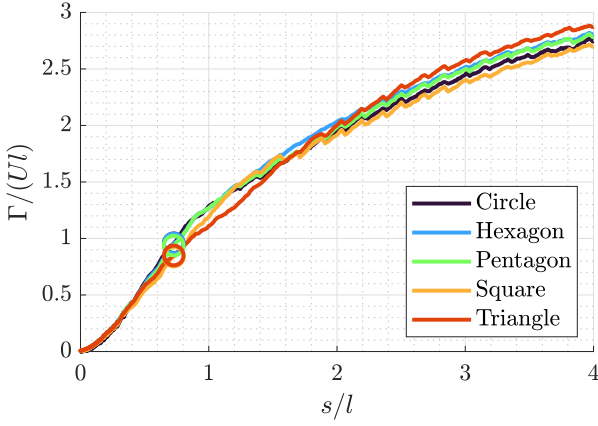
2

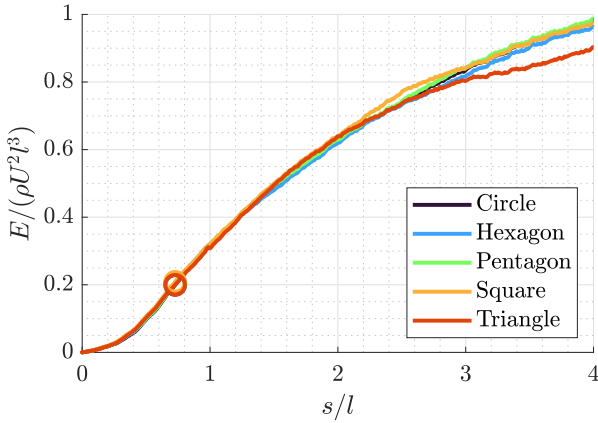Figure 3. Circulation Γ of flow field behind each plate.

Figure 4. Kinetic energy E of flow field behind each plate.

the field.

Kinetic Energy

Kinetic energy E behind each plate is plotted in fig. 4. Kinetic is calculated by performing a volumetric integral on the absolute velocity of the flow field behind each plate, over all measured angles of φ.

While the kinetic energy behinds all plate collapses to the same curve for all plates over distances travelled of $s/l \in [0,3]$, the kinetic energy of the flow behind the triangular plate drops off beyond $s/l > 3$, while all other kinetic energy profiles remain consistent. The reduction in kinetic energy behind the triangular disk could be associated with the dissipation of kinetic energy, as the vortex loop behind the triangular disk may begin breaking down to turbulence. An investigation into the vorticity distribution behind each plate is necessary to better understand the underlying phenomena.

Vorticity Distribution

Figure 5 displays snapshots of the vorticity field from a single run when the plate has travelled distances of $s/l = 0.5, 1.5$, and 3.0. Three cases are displayed: around a circular plate (left), and triangular plates at $\varphi = 0°$ (centre) and $\varphi = 30°$ (right). In the case of the circular plate, the snapshots show a pair of counter-rotating vortices that remain symmetric and circular. As the plate travels along, the vortices grow in size, but snapshots still contain a pair of distinct, circular, coherent primary vortices by $s/l = 3$. Similar results were found

for all runs at all tested azimuthal planes φ behind the circular plate.

In the case of the triangular plate, along the $\varphi = 0°$ plane, while the pair of vortices remains symmetric, they no longer remain circular as they breakdown. At $s/l = 1.5$, the vortices appear stretched and no longer have distinct circular contours, and by $s/l = 3$, they are mostly broken down. In the case of planes of non-symmetric cross-sections, such as the $\varphi = 30°$ plane, the vortex loop is not symmetric, with the vortex trailing closely behind the triangle's point, while lagging further behind its flat edge. These characteristics are consistent with the flow visualizations of Higuchi *et al.* (1996). By $s/l = 3$, the vortex loop is stretched out into patches of vorticity, and no longer contains clear, distinct vortices in any measured azimuthal plane φ.

Snapshots behind the square plate are shown in fig. 6. Similar to the results of the circular plate, there is a distinct pair of vortices at all snapshots. However, the vortices behind the square plate are less coherent than those behind the circle at similar distances travelled. By $s/l = 3$, the vortex loop is showing signs of breakdown, as each vortex is stretched out. While all cross-sectional planes behind the square plate are symmetric, comparing planes at different azimuthal angles shows that the vortex loop is not axisymmetric. Similar to the triangle, and the findings of Higuchi *et al.* (1996), the vortex loop trails closely behind the plate along its vertices ($\varphi = 45°$), while it lags further behind the plate along its flat edges ($\varphi = 0°$). This phenomenon is most prevalent in the case of the triangular plate, which has the sharpest edge discontinuities.

While visually it is evident that the vortex loop behind the triangular disk breaks down to turbulence quicker than behind the circular disk, traditional quantifiable values for the flow field, such as circulation and kinetic energy, show no difference. A quantifiable metric would be useful to evaluate loop coherence. One such metric is proposed and tested on the current dataset in the following section.

COHERENCE OF VORTEX LOOPS

To quantify the coherence of the vortex loop, we propose a coherence metric of

$$C_{12} = \frac{1}{\Delta\varphi_{\max}} \int_0^{\Delta\varphi_{\max}} C_{12}(\Delta\varphi)\mathrm{d}(\Delta\varphi), \qquad (1)$$

in which $C_{12}(\Delta\varphi)$ is the 2-dimensional correlation coefficient between two vorticity fields ω_1 and ω_2, each separated by an angle $\Delta\varphi$. A perfectly axisymmetric vortex ring will return a coherence value of $C_{12} = 1$ at any given time, while a fully turbulent wake, with zero correlation between any azimuthal planes, should have $C_{12} = 0$.

This metric is similar to the approach of Johansson *et al.* (2002), who found the correlation $C_{12}(f, \Delta\varphi)$ of hot-wire at various angles of azimuthal separation to measure the coherence of azimuthal modes in steady wakes. In the absence of steady-state, high-frequency hot-wire measurements, we use image correlations over several repeated runs, integrating over all degrees of separation $\Delta\varphi$, to quantify the loop coherence at each timestep.

Vortex loop coherence for each plate is shown in fig. 7. Specifically, the vorticity fields on each half-plane, for $(r,x) \in [0,l] \times [-0.25l, x_{\text{plate}}]$, are used to calculate the correlation between planes at all measured azimuthal planes φ.
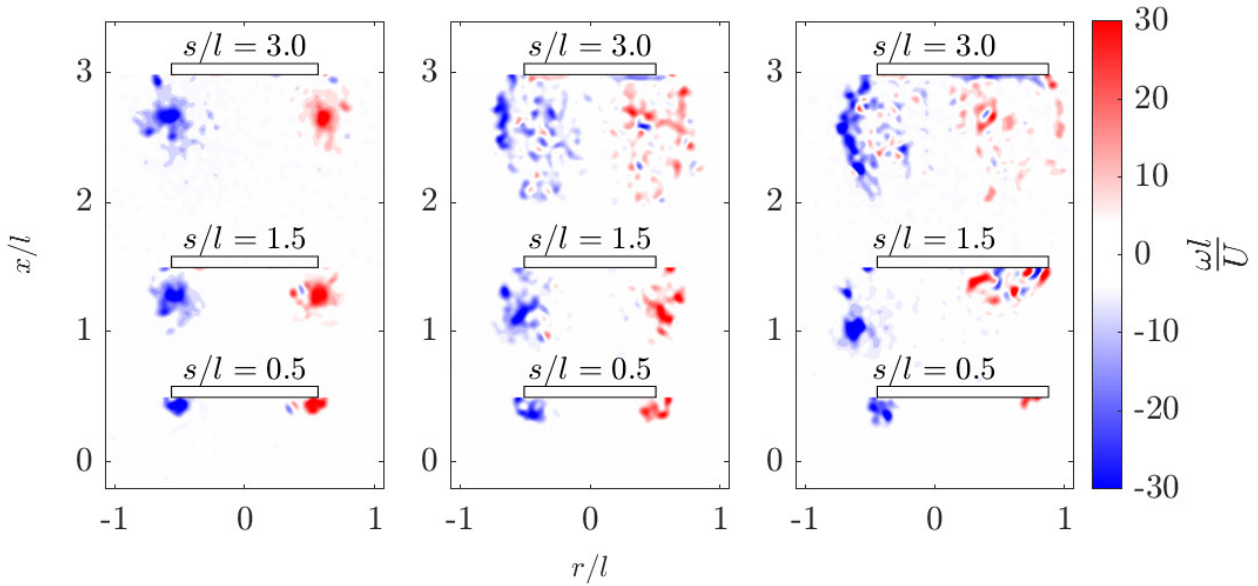
Figure 5.   Snapshots of vortex evolution behind circular plate (left), and triangular plates at $\varphi = 0°$ (centre) and $\varphi = 30°$ (right).
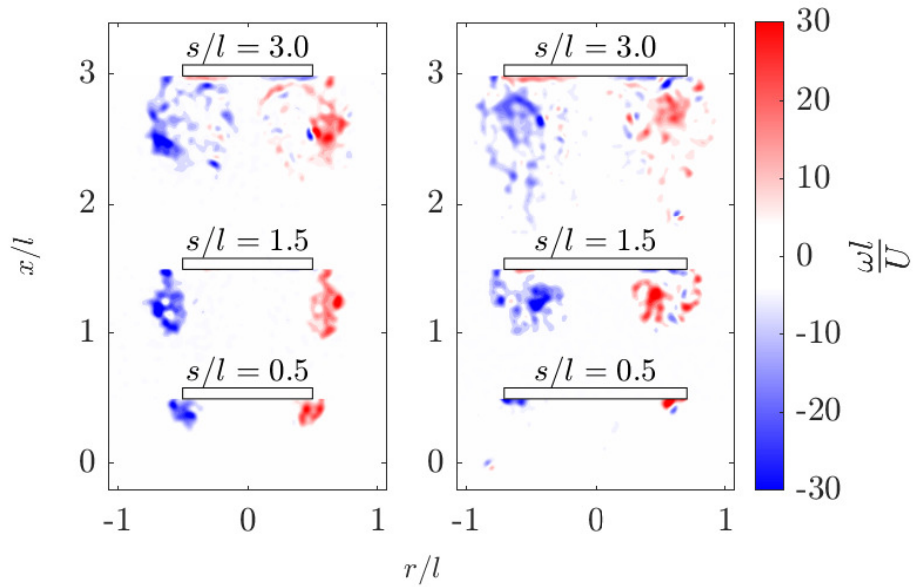

Figure 6.   Snapshots of vortex evolution behind square plate at $\varphi = 0°$ (left) and $\varphi = 45°$ (right).
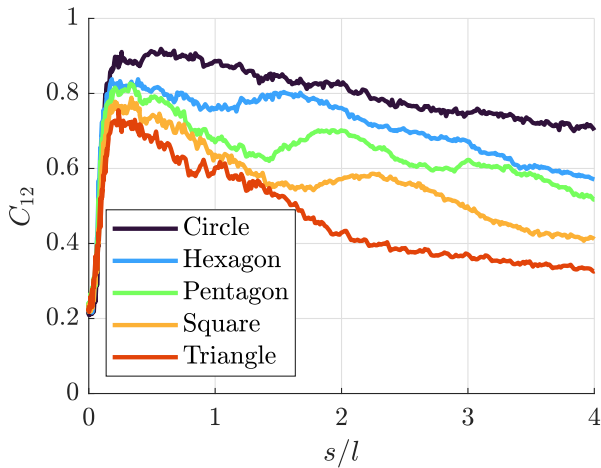

Figure 7.   Vortex loop coherence evolution behind each plate.

All vortex loops achieve their peak coherence at small distances travelled, around $s/l = 0.25$, after which they gradually decay. The circular disk has the highest peak loop coherence of $C_{12} = 0.91$, while the peak loop coherence decreases with increasing plate perimeter, as the triangular disk has the smallest value, at $C_{12} = 0.76$. At a distance travelled of $s/l = 3$, the circular plate has a loop coherence of $C_{12} = 0.75$, while the triangular plate has a loop coherence of $C_{12} = 0.37$. At $s/l = 1.5$, where the loop behind the triangular disk is clearly deformed, $C_{12} = 0.52$. Comparing results to the vorticity snapshots in fig. 5, decreasing values of C_{12} appear to be a sign of vortex breakdown.

At all distances travelled, the vortex loop behind the circular disk had the highest coherence, followed by the loops behind the hexagonal, pentagonal, square, and triangular plates, respectively. With constant plate area, loops are less coherent behind plates with larger perimeters and sharper discontinuities. After nearly four characteristic lengths travelled, the cir-

4

cular plate's coherence value is still higher than the peak value behind the triangular disk.

In addition to the peak coherence, the drop in loop coherence is steeper for plates with larger perimeters. After travelling $s/l = 4$, C_{12} decreases by 0.20 for the circular plate, while it decreases by 0.33 over the same distance for the triangular plate.

We propose that a coherence value around $C_{12} = 0.5$ is a reasonable threshold, below which the transition to turbulence begins in vortex loops. Of the measured plates, only the vortex loops behind square and triangular vortex loops cross below this threshold. The square plate crosses below this threshold around $s/l = 3.0$, while the triangular plate crosses this threshold earlier, around $s/l = 1.6$. The full breakdown of vortex rings towards turbulent wakes appear to be associated with lower coherence values, around $C_{12} = 0.35$, which is only observed in the triangular plate, around $s/l = 3.3$, and will occur beyond $s/l > 4$ in other polygonal and circular plates.

CONCLUSIONS

In this work, we examined the coherence of vortex loops generated by impulsively-started flat plates of various geometries. While plate geometry plays a minor role in circulation and kinetic energy of the resultant flow field, it plays a major role on the distribution of vorticity. This altered vorticity distribution leads to less coherent vortex loops, which, in turn, break down faster.

Using a coherence metric C_{12}, we found that loop coherence is consistently higher for plates with smaller perimeters. The sharp discontinuities in low-order polygons, such as triangles and squares, are associated with lower peak values of C_{12}, and steeper decreases in C_{12} than geometries with smaller perimeters and smoother geometries, such as circles and hexagons. This decrease in C_{12} indicates the faster break-down in vortex loops towards turbulence behind plates with sharper discontinuities. Coherence metric values can be used to identify critical transition points of vortex loops, with transition to turbulent vortex loops occurring around $C_{12} = 0.50$, and vortex loop breakdown occurring around $C_{12} = 0.35$.

REFERENCES

Fernando, J. N. & Rival, D. E. 2016 On vortex evolution in the wake of axisymmetric and non-axisymmetric low-aspect-ratio accelerating plates. *Physics of Fluids* **28** (1).

Fernando, J. N., Weymouth, G. D. & Rival, D. E. 2020 On the limits of added-mass theory in separated flows and with varying initial conditions. *Journal of Fluids and Structures* **93**.

Ghasemi, Abbas, Roussinova, Vesselina & Balachandar, Ram 2013 A study in the developing region of square jet. *Journal of Turbulence* **14** (3), 1–24.

Grinstein, F. F. & DeVore, C. R. 1996 Dynamics of coherent structures and transition to turbulence in free square jets. *Physics of Fluids* **8** (5), 1237–1251.

Gutmark, E. J. & Grinstein, F. F. 1999 Flow control with non-circular jets. *Annual review of fluid mechanics* **31** (1), 239–272.

Higuchi, H., Anderson, R. W. & Zhang, J. 1996 Three-dimensional wake formations behind a family of regular polygonal plates. *AIAA Journal* **34** (6), 1138–1145.

Johansson, P. B. V., George, W. K. & Woodward, S. H. 2002 Proper orthogonal decomposition of an axisymmetric turbulent wake behind a disk. *Physics of Fluids* **14** (7), 2508–2514.

Nedić, J., Supponen, O., Ganapathisubramani, B. & Vassilicos, J. C. 2015 Geometrical influence on vortex shedding in turbulent axisymmetric wakes. *Physics of Fluids* **27** (3), 35103.